Chinese Journal of
POLYMER SCIENCE

RESEARCH ARTICLE

https://doi.org/10.1007/s10118-026-3730-6
Chinese J. Polym. Sci.

Low-cost Preparation of High-performance Polyimide Separators: High-value Application of Recycled Polyimide Films

Ying-Hua Sha[a], Zi-Hao Huang[a], Jia-Shu Lin[a], Yan-Wei He[c], Chu-Ying Li[a], Hai-Tao Huang[a,b*], Si-Wei Liu[a*], and Yi Zhang[a*]

[a] *PCFM Lab, GD HPPC Lab, Guangdong Engineering Technology Research Centre for High-performance Organic and Polymer Photoelectric Functional Films, GBRCE for Functional Molecular Engineering, State Key Laboratory of Optoelectronic Materials and Technologies, School of Chemistry, IGCME, Sun Yat-sen University, Guangzhou 510275, China*
[b] *Key Laboratory of Guangdong Higher Education Institutions of Northeast Guangdong New Functional Materials, School of Chemistry and Environment, Jiaying University, Meizhou 514015, China*
[c] *Wuxi Shunxuan New Materials Co., Ltd., Wuxi 214037, China*

Electronic Supplementary Information

Abstract With growing global focus on plastic circular recycling and sustainable development, chemical upcycling is gaining importance. It converts waste plastics into high-value products, avoiding the performance degradation and downcycling associated with conventional physical recycling processes. Polyimide (PI) is a high-performance polymer material, particularly valued in the field of lithium-ion batteries as a separator due to its high-temperature resistance, favorable mechanical strength, and good electrolyte wettability. However, its broader application has been limited by the high cost of its monomers and the energy consumption of its preparation process compared to conventional lithium-ion battery separators such as polyethylene/polypropylene. Here, we propose an effective strategy for the high-value application of recycled polyimide (PMDA/ODA-type) films through chemical catalysis: using lithium hydroxide to catalyze the partial ring-opening of the imide rings in recycled polyimide, transforming the insoluble and infusible recycled polyimide into a soluble poly(amic acid)-polyimide system (PAA-PI). This system is further processed *via* electrospinning to fabricate polyimide nanofiber membranes, which are applied as separators in lithium-ion batteries. They exhibit similar structural, thermal properties, and mechanical properties to the PI separators prepared by the traditional method, while also possessing good porosity, electrolyte wettability, and electrolyte uptake. Furthermore, batteries prepared using this recovered PI separator (RPI) exhibit excellent high-rate performance (135.55 mAh·g^{-1} at 5 C current) and long-term cycle stability (118.01 mAh·g^{-1} after 100 cycles at 0.5 C current, and 87.10 mAh·g^{-1} after 100 cycles at 2.0 C current), showing no significant difference compared to batteries prepared with conventional PI separators, while outperforming batteries prepared with commercial Celgard 2500 separators, essentially meeting the performance requirements of next-generation lithium-ion batteries. This work presents a strategy for the low-cost production of high-safety polyimide-based separators in lithium-ion batteries, enabling the high-value reuse of polyimide waste and thereby establishing a process consistent with green chemistry and sustainable development.

Keywords Recycled polyimide; Chemical upcycling; Lithium-ion batteries; Separator; Partial ring-opening

Citation: Sha, Y. H.; Huang, Z. H.; Lin, J. S.; He, Y. W.; Li, C. Y.; Huang, H. T.; Liu, S. W.; Zhang, Y. Low-cost preparation of high-performance polyimide separators: high-value application of recycled polyimide films. *Chinese J. Polym. Sci.* https://doi.org/10.1007/s10118-026-3730-6

INTRODUCTION

Polyimides are a class of aromatic heterocyclic polymers containing imide rings in their molecular structures. They possess excellent properties, such as high thermal stability, high strength, high modulus, good chemical resistance, high electrical insulation, and low dielectric constant,[1–4] and are widely used in various fields, including aerospace,[5,6] flexible displays,[7,8] liquid crystals,[9,10] electronic packaging,[11,12] and batteries.[13,14] It is noteworthy that the electrochemical properties of PI are important for the development of energy storage and conversion technologies.[15] In particular, in the field of lithium-ion batteries, the multifunctional characteristics and reliability of PI make it a promising material for addressing the challenges of next-generation lithium-ion batteries in terms of energy density, safety, and lifespan.

The separator is a key component in lithium-ion batteries. Currently, traditional polyolefin separators have low melting points and poor thermal stability. In addition, the nonpolar nature of polyolefins leads to poor electrolyte wettability and low ionic conductivity. Researchers have been dedicated to

* Corresponding authors, E-mail: huanght36@mail2.sysu.edu.cn (H.T.H.)
E-mail: liusiw@mail.sysu.edu.cn (S.W.L.)
E-mail: ceszy@mail.sysu.edu.cn (Y.Z.)
Received May 11, 2026; Accepted May 26, 2026; Published online September 1, 2026

© Chinese Chemical Society
Institute of Chemistry, Chinese Academy of Sciences

finding a new generation of separators with excellent thermal stability. Among them, PI separators meet almost all the requirements and can effectively address critical challenges such as poor thermal stability, low ionic conductivity, and lithium dendrite growth in lithium-ion batteries, helping to extend the lifespan and efficiency of lithium-ion batteries.[16] However, the high cost of raw materials and processing limits the practical application of PI separators.

However, the recycling and reuse of PI materials are expected to address this issue. Currently, there are three common recycling methods for PI materials, as shown in Fig. 1. The first method (Fig. 1a) involves crushing PI waste into a powder or small flakes to be blended with PI or other matrix polymers to fabricate polymer composites.[17–19] This method is simple to operate, inexpensive, and time-efficient. However, there are certain limitations in processing and molding techniques as well as in product performance, making it difficult to achieve high-value recycling. The second method (Fig. 1b) involves high-temperature pyrolysis, in which useful synthesis gases and carbon materials can be recovered from PI materials without the need for added catalysts or organic solvents.[20,21] For example, the high-temperature treatment of polyimide has been used to develop large-area, high-quality graphite films. This process consumes considerable energy, is costly, and may produce toxic gases that cause secondary pollution. The third method (Fig. 1c) involves degrading polyimide in acidic or alkaline solutions to recover diamine or dianhydride monomers. After purification, these monomers can be resynthesized into polyimide, thereby achieving closed-loop recycling.[22–24] However, side reactions may occur during this process, and the subsequent purification procedures are complex, costly, and time-consuming.

In recent years, researchers have proposed a chemical upcycling strategy,[25] a method to convert plastic waste into value-added chemicals and materials, which has become a promising approach to addressing issues such as plastic waste. For instance, Chen *et al.*[26] upcycled discarded thermosetting polyimide resins into high-performance and sustainable low-temperature adhesives, achieving upgraded recycling of PI materials. Cai *et al.*[27] developed a new approach to prepare high value-added thermal insulation aerogel materials from waste PET using mechanochemical methods, making it an ideal raw material for aerogel production. In contrast to common recycling methods, chemical upcycling strategies are more selective and consume less energy. In recent years, as environmental pressure from plastic waste has gained increasing attention, chemical upcycling strategies have played a crucial role in the recycling of plastics and the sustainable development of resources.

In this study, we propose a new method (Fig. 1d) for preparing battery separators based on PI (PMDA/ODA-type) film waste generated during industrial production. This method uses lithium hydroxide to partially break the imide rings in the PI, yielding a soluble polyimide precursor, poly(amic acid)-polyimide (PAA-PI) solution, which is then processed into polyimide lithium battery separators (RPI separators) *via* electrospinning. Throughout the process, the original PI did not degrade into monomers, making the approach both simple and environmentally friendly. The RPI separators derived from the PAA-PI solution exhibited similar morphology and performance to those prepared from monomers using the conventional two-step method, and the assembled symmetric cells demonstrated excellent battery performance. This study enables low-cost fabrication of polyimide-based battery separators while achieving high-value reutilization of polyimide waste, aligning with the principles of green chemistry and sustainable development.

EXPERIMENTAL

Materials

The waste PI produced during the industrial production of PI

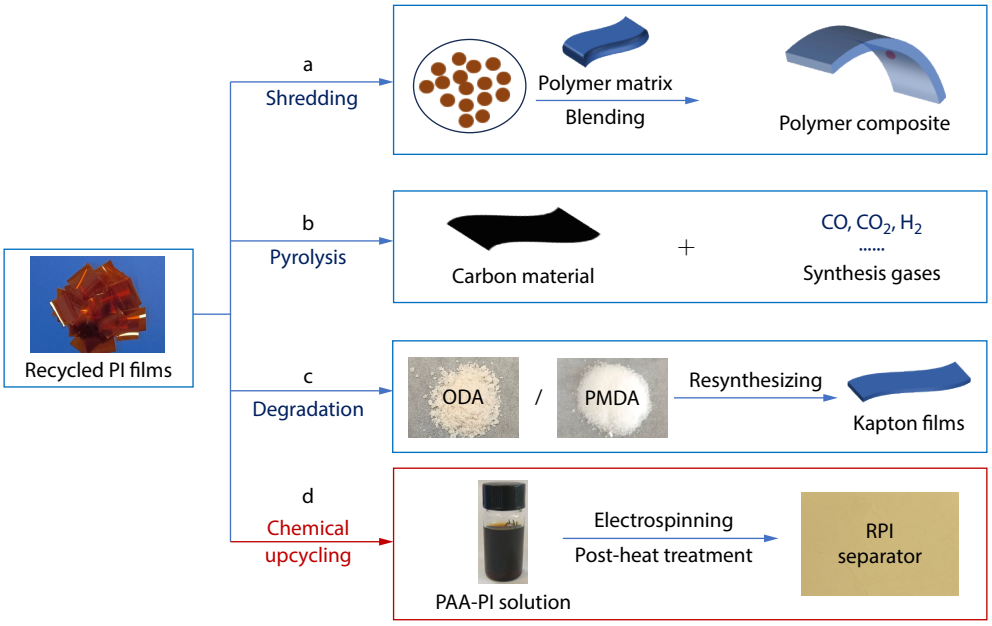

Fig. 1 Schematic diagram of various recycling routes for polyimide waste films.

films (rPI) was supplied by Wuxi Shunxuan New Materials Co., Ltd. Lithium hydroxide (LiOH) was purchased from Anhui Zesheng Technology Co., Ltd. *N*,*N*-Dimethylformamide (DMF, >99%) was purchased from J&K Scientific Co., Ltd. Li foil, $LiCoO_2$ and 1.0 mol·L^{-1} $LiPF_6$ in ethylene carbonate/diethyl carbonate/dimethyl carbonate (EC/DEC/DMC, 1/1/1, *V*/*V*/*V*) were provided by Guangdong City New Energy Technology Co., Ltd. Pyromellitic dianhydride (PMDA, >99.5%) and 4,4'-diaminodiphenyl ether (ODA, >99.5%) were purchased from China Tech (Tianjin) Chemical Co., Ltd. For comparison, a Celgard 2500 separator with a PP/PE/PP three-layer structure was obtained from Celgard LLC (USA).

Preparation of PAA-PI Solution by Controlled Partial Open-loop Process of rPI

Before the experiment, the rPI samples were cleaned with ethanol, dried, and cut into 15 mm × 15 mm squares for subsequent use. The hydrolysis of rPI was carried out in a 250 mL beaker. rPI (10 g) was added to a 250 mL beaker containing 200 g of LiOH solution (10 wt%) and stirred with a magnetic stirrer for 15 h. The mixture was then filtered to separate the solid residues of the rPI fragments, which were subsequently washed with 500 mL of 2 mol·L^{-1} hydrochloric acid for 30 min. To remove the residual acid, the solid residues were ultrasonically cleaned in deionized water for 1 h and repeatedly rinsed until the wash solution was nearly neutral. The obtained solid residues were dried at 50 °C for 8 h. Then, 10 g of the dried rPI fragments was dissolved in 20 mL of DMF to prepare a recycled PAA-PI solution with a solid content of 35 wt%.

Preparation of RPI Separators by Electrospinning

The corresponding battery separators were fabricated using electrospinning. The specific process was as follows: PAA-PI solution (5 g, 35 wt% in DMF) was added to a 10 mL syringe. Electrospinning was conducted at an applied voltage (+15 kV, −5 kV) using a syringe needle with an inner diameter of 0.5 mm. The solution was fed at a constant rate of 1 mL·h^{-1}, and the working distance between the needle tip and collector was set to 20 cm. The electrospinning process was maintained for 3 h to obtain the nanofiber membranes. The resulting separators were then heat-treated in an oven under an air atmosphere at a heating rate of 5 °C·min^{-1} to 350 °C, and held at this temperature for 60 min, yielding polyimide nanofiber separators (denoted as RPI separators). For comparison, a control PI nanofiber separator was prepared following the same procedure, using a poly(amic acid) (PAA) precursor synthesized directly from the monomers (PMDA and ODA).

Half-cell Assembly

Coin-type half-cells (CR2025) were assembled in an argon-filled dry glove box under inert atmosphere. Three types of separators were used: Celgard 2500, PI, and RPI. Lithium foil served as the anode and $LiCoO_2$ (with an areal mass loading of 10.21 mg·cm^{-2}) was used as the cathode. The electrolyte was 1.0 mol·L^{-1} $LiPF_6$ dissolved in a mixture of ethylene carbonate (EC), diethyl carbonate (DEC), and dimethyl carbonate (DMC) at a 1:1:1 volume ratio.

Characterization

Attenuated total reflectance Fourier-transform infrared (ATR-FTIR) spectra were recorded using a Bruker TENSOR 27 spectrometer over the range of 500–4000 cm^{-1}. X-ray photoelectron spectroscopy (XPS) was performed using a Nexsa (Thermo Fisher Scientific) instrument with a pass energy of 40.0 eV and a spectral integration value of 441. Molecular weights were determined by gel permeation chromatography (GPC, Waters e2695) using DMF containing 0.05 mol·L^{-1} LiBr as the eluent and calibrated with poly(methyl methacrylate) (PMMA) standards. The surface morphology of the fibrous separator samples was examined by scanning electron microscopy (SEM, Hitachi S4800). Thermogravimetric analysis (TGA) was performed on a Netzsch TGA209F1 instrument under a nitrogen atmosphere from 40 °C to 800 °C at a heating rate of 10 °C·min^{-1}. The fatigue resistance of the specimens (10 mm × 50 mm) was evaluated using a flexible-display folding-endurance tester (PT-604A, Guangdong Beidou Precision Instrument Co., Ltd.) at a fixed bending radius of 4 mm over 1×10^5 folding-unfolding cycles. Dynamic mechanical properties of the specimens (10 mm × 20 mm) were measured using a TA instrument DMA Q800 in tensile mode at 25 °C. The electrolyte contact angles of the samples (10 × 10 mm) were characterized using an optical contact angle analyzer (KRUSS K12) with a droplet deposition time of approximately 1000 ms. The porosity, electrolyte uptake characterization of the separators, and electrochemical measurements are provided in the electronic supplementary information (ESI).

RESULTS AND DISCUSSION

Controlled Partial Open-loop Process of rPI to Soluble PAA-PI

NaOH is widely used as a catalyst in the degradation of PI because it can rapidly decompose PI into its constituent dianhydride and diamine monomers at elevated temperatures.[28] Similarly, LiOH exhibited a comparable effect. However, LiOH (pK_b=0.18) is less alkaline than NaOH (pK_b=−0.56), resulting in a relatively lower catalytic activity, thus enabling a milder and more controllable degradation process. Additionally, the smaller ionic radius of lithium facilitates more selective attack on specific chemical bonds. For battery materials derived from recovered products, residual lithium ions are also more readily accommodated than sodium ions. Therefore, LiOH was selected as the catalyst for this study. By controlling the reaction time at room temperature, the imide bonds in the PI were cleaved to yield a lithium polyamate intermediate. Hydrochloric acid was then introduced as an acidifying agent to convert lithium polyamates into polyamide acid. After washing with deionized water to remove residual acid, the product was dried and dissolved in DMF to prepare the recycled PAA-PI solution.

Fig. 2 shows digital images of the rPI films immersed in a 10 wt% LiOH solution for 5, 10, and 15 h, followed by sequential washing with hydrochloric acid and deionized water, followed by drying. The solubility of the resulting samples was evaluated by immersing 20 mg of each sample in 2 mL of DMF. It was observed that the samples immersed for 5 and 10 h remained almost insoluble in DMF, whereas the sample immersed for 15 h completely dissolved, forming a transparent solution. The infrared spectra (Figs. 3a and 3b) demonstrate the partial ring-opening of rPI films treated with LiOH for different durations (rPI-*x* denotes rPI films after soaking in a 10 wt% LiOH solution for *x* h, followed by washing with hydrochloric acid and deionized water, and drying). As the immersion time increased, the characteristic imide peaks of the

treated samples gradually diminished and the intensities of the amide-related peaks progressively increased. Specifically, the amide I band (C=O stretching) appeared at about 1650 cm^{-1}, the amide II band (coupled N–H bending and C—N stretching vibrations) at about 1540 cm^{-1}, and the amide III band (C—N stretching vibration) at about 1211 cm^{-1}. Moreover, as shown in Table S1 (in ESI), no lithium was detected in rPI-15, indicating that lithium ions were completely removed during the hydrochloric acid washing step. These results provide direct evidence for the formation of amide structures, confirming that partial and controllable ring-opening of polyimide occurred, leading to the coexistence of poly(amic acid) and polyimide. Therefore, 15 h was selected as the optimal experimental time for preparing the soluble polyimide pre-

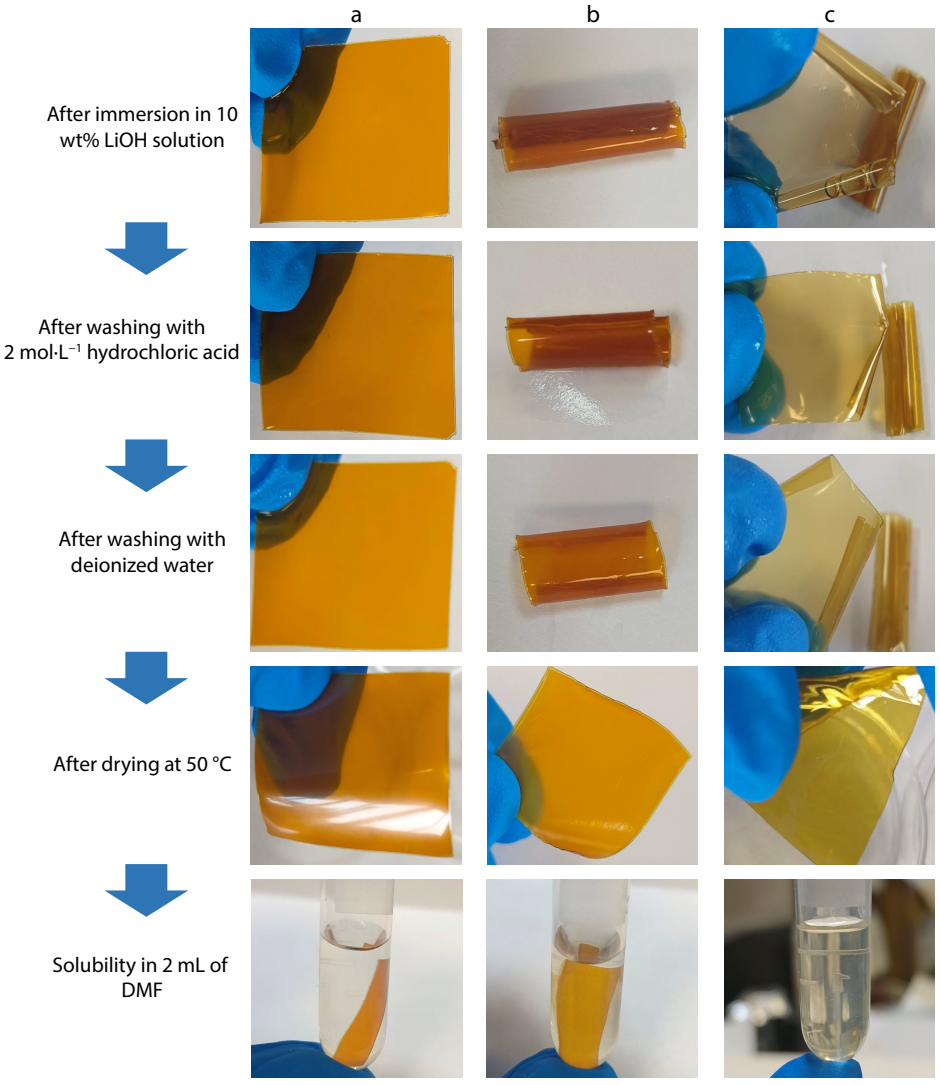

Fig. 2 Digital pictures of the rPI films immersed in 10 wt% LiOH solution at room temperature for different durations: (a) 5 h, (b) 10 h, and (c) 15 h at different stages.

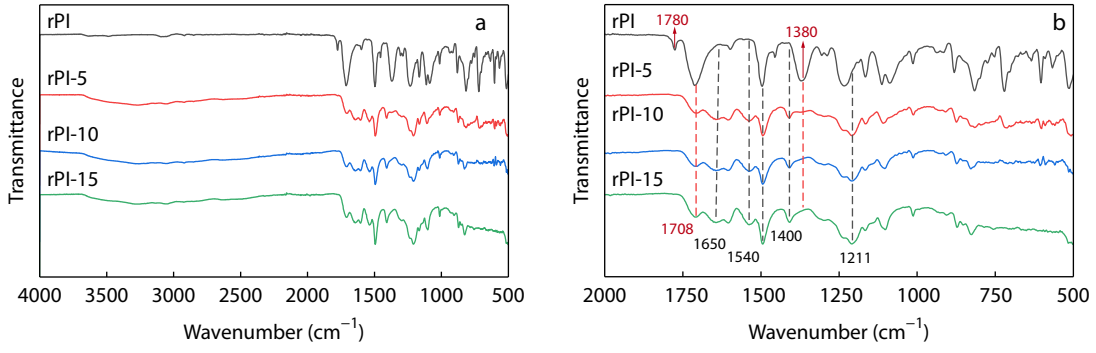

https://doi.org/10.1007/s10118-026-3730-6

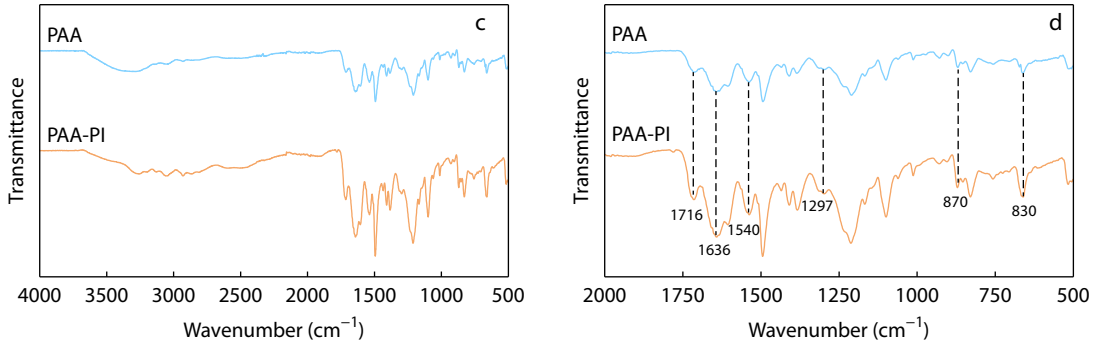

Fig. 3 (a) FTIR spectra of rPI films after immersion in 10 wt% LiOH for different durations; (b) FTIR spectra of (a) enlarged from 500 cm^{-1} to 2000 cm^{-1}; (c) FTIR spectra of PAA and PAA-PI solution; (d) FTIR spectra of (c) enlarged from 500 cm^{-1} to 2000 cm^{-1}.

cursor.

A comparison of the FTIR spectra of PAA and the recycled polyimide precursor solution (Figs. 3c and 3d) reveals similar characteristic bands for both materials. The peak at 1716 cm^{-1} represents the carbonyl (C=O) stretching vibration of the carboxyl group (—COOH). The peaks at 1636, 1540, and 1297 cm^{-1} correspond to amide I (C=O stretching), amide II (coupled C—NH bending), and amide III (C—N stretching) vibrations, respectively. The peaks observed at 1498 cm^{-1} and 830–875 cm^{-1} are characteristic of aromatic rings. These spectral features indicate that the structure of the recycled solution is consistent with that of PAA and polyimide. In addition, GPC analysis (Table S2 in ESI) showed that the molecular weight of the PAA-PI solution exceeded 24000 g·mol^{-1}, suggesting favorable processability.

Structural Characterization of RPI Separators

Using different PAA-based solutions, PMDA/ODA-type PI nanofiber separators (controlled) and RPI nanofiber separators were fabricated *via* electrospinning. The FTIR spectra of both separators (Fig. 4) exhibit characteristic absorption peaks corresponding to the imide ring: asymmetric and symmetric C=O stretching vibrations at 1780 and 1708 cm^{-1}, respectively, along with the C—N stretching vibration at approximately 1380 cm^{-1}. These results confirmed that the RPI nanofiber separators retained the structural features typical of conventional PI separators. Moreover, the SEM images (Fig. 5) show no significant morphological differences between the two types of separators prepared using the different methods.

Mechanical Properties of RPI Separators

The mechanical strength of the separator is crucial for suppressing the growth of lithium dendrites and ensuring compatibility with battery manufacturing processes. As shown in Fig. 6, after 1×10^5 bending tests (Fig. S1 in ESI), neither the PI nor the RPI separators exhibited visible cracks, indicating their excellent bending resistance and deformation tolerance. In addition, the tensile strengths of the PI and RPI separators obtained from DMA tests were 21 and 17 MPa, respectively. Moreover, the tensile strength of the RPI separator remained virtually unchanged after the fatigue testing (Fig. S2 and Table S3 in ESI). Although both separators exhibited excellent mechanical properties, the

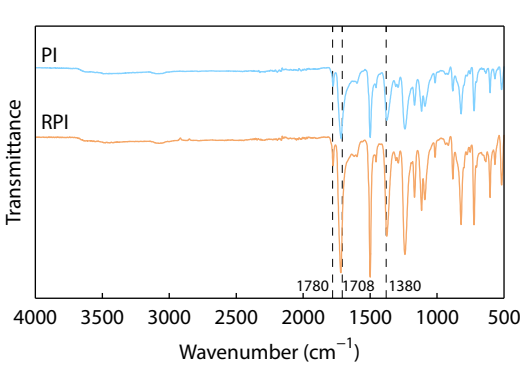

Fig. 4 FTIR spectra of PI and RPI separators.

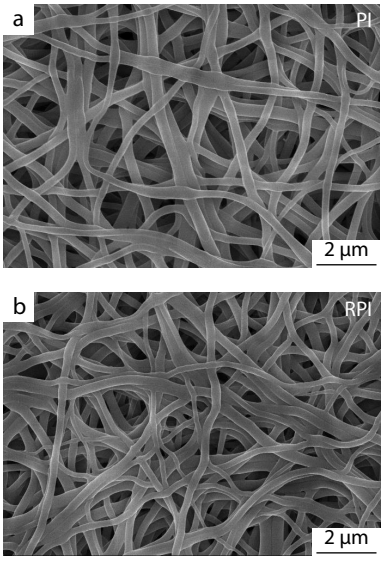

Fig. 5 SEM images of PI separator (a) and RPI separator (b).

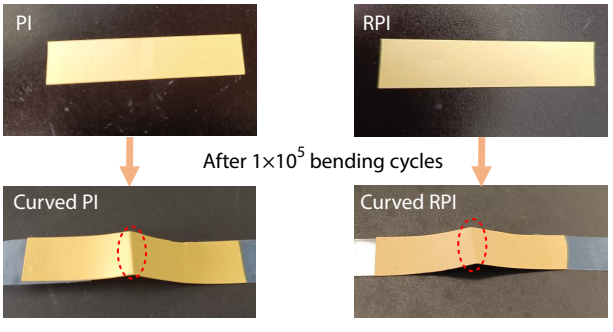

Fig. 6 Digital pictures of PI and RPI separators before and after 1×10^5 fatigue resistance tests.

https://doi.org/10.1007/s10118-026-3730-6

RPI separator showed a slight reduction in tensile strength compared with the pristine PI separator, which can be attributed to the decrease in molecular weight during the alkali treatment process. Nevertheless, the RPI separator retained excellent mechanical integrity, making it suitable for battery applications.

Thermal Properties of RPI Separators

The thermal resistance of the RPI separator was evaluated by TGA (Fig. 7a). Although the RPI separator exhibited slightly lower thermal performance compared to the pristine PI separator, it still maintained good thermal stability, with a 1% weight loss temperature ($T_{1\%}$) of 413 °C. Additionally, excellent thermal dimensional stability is essential for preventing safety hazards caused by direct contact between the cathode and anode, resulting from thermal shrinkage of the separators at elevated temperatures. To assess this property, the thermal shrinkage behavior of various separators was examined at different temperatures. Fig. 7(b) shows photographs of the Celgard 2500, PI, and RPI separators after being held at various temperatures for 30 min. The results showed that the Celgard 2500 separator began to shrink at 100 °C, became a translucent film at 150 °C, and turned yellow, and melted into a clump at 200 °C. In contrast, both the PI and RPI separators exhibited no significant shrinkage or color change, even after annealing at 200 °C for 30 min, which can be attributed to the excellent high-temperature resistance inherent to the polyimide structure. The above results demonstrate that both the PI and RPI separators possess outstanding thermal resistance and further confirm their structural similarity.

Wettability, Electrolyte Absorption, and Porosity of RPI Separators

To evaluate the electrolyte wettability of the separators, contact angle tests using the liquid electrolyte were conducted on different separators (Fig. 8a). The contact angles of the electrolyte on the Celgard 2500, PI, and RPI separators are 39.5°, 13.6°, and 13.5°, respectively. Compared with non-polar polyolefin materials, the polar nature of polyimide materials endows them with greater affinity for the electrolyte, resulting in a smaller contact angle. The contact angle of the RPI separator is comparable to that of the PI separator, indicating the similar polarity of the materials obtained *via* the two different preparation methods. Furthermore, as shown in Fig. 8(b), both PI and RPI separators exhibit substantially higher electrolyte uptake than Celgard 2500, although RPI shows slightly lower uptake than the pristine PI separator. As summarized in Table S3 (in ESI), the two separators had comparable porosities, both exceeding that of Celgard 2500.

Electrochemical Performance of RPI Separators

In the Nyquist plot shown in Fig. 9(a), the intercept of the curve with the real axis (Z') corresponds to the volume resistance of the separator. The results indicate that the bulk resistances (R_b) of the RPI and PI nanofiber separators are comparable, measur-

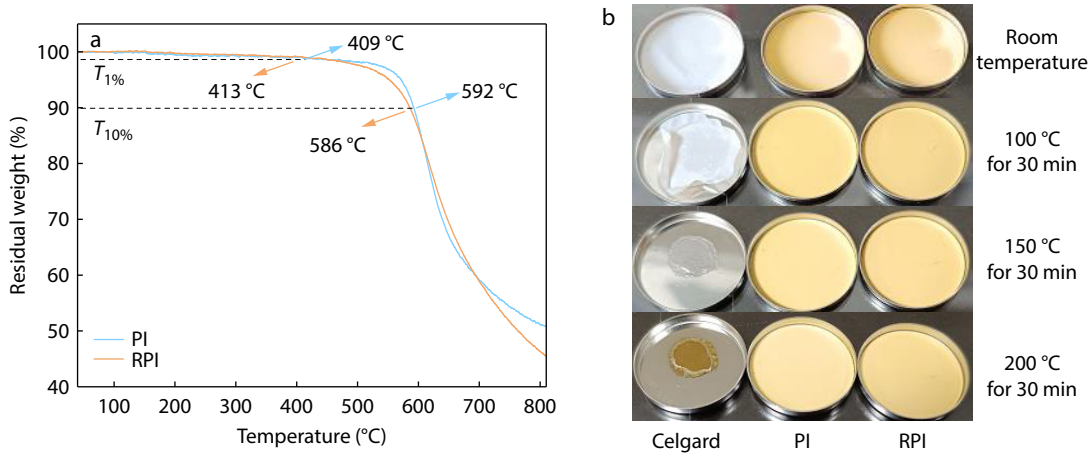

Fig. 7 (a) The TGA curves of different separators under N_2 atmosphere; (b) Digital pictures of the Celgard 2500, PI and RPI separators at different temperatures.

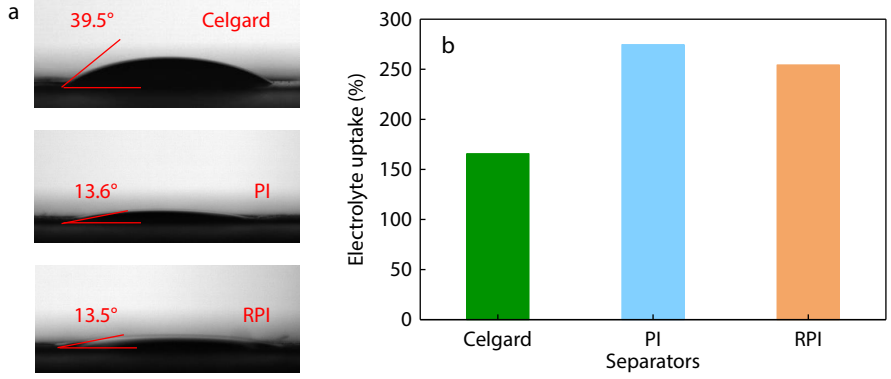

Fig. 8 Contact angle (a) and electrolyte uptake (b) of Celgard 2500, PI, and RPI separators with the electrolyte.

https://doi.org/10.1007/s10118-026-3730-6

ing 3.27 Ω and 2.68 Ω respectively, both lower than that of the Celgard 2500 (5.97 Ω). The ionic conductivities (σ) of the Celgard 2500, PI, and RPI separators are shown in Fig. 9(b) and Table 1. Compared to the Celgard 2500 separator (0.21 mS·cm^{-1}), both the RPI (0.67 mS·cm^{-1}) and PI (0.76 mS·cm^{-1}) separators exhibit higher ionic conductivity, which can be attributed to their higher porosity arising from the nanofibrous structure.

The lithium-ion transference number is another important parameter for evaluating separator performance, with higher values being beneficial for improving the rate capability of lithium-ion batteries. Electrochemical impedance spectroscopy (EIS) is an effective method for investigating the lithium-ion diffusion behavior.[29] The semicircle in the EIS spectrum corresponds to the interfacial resistance associated with lithium-ion migration. The interfacial resistance (R_{SEI}) derived from EIS is inversely correlated with the lithium-ion transference number, as a lower resistance facilitates faster Li^+ transport across the interface. The interface resistances of the PI and RPI separators were 264 and 274 Ω, respectively,

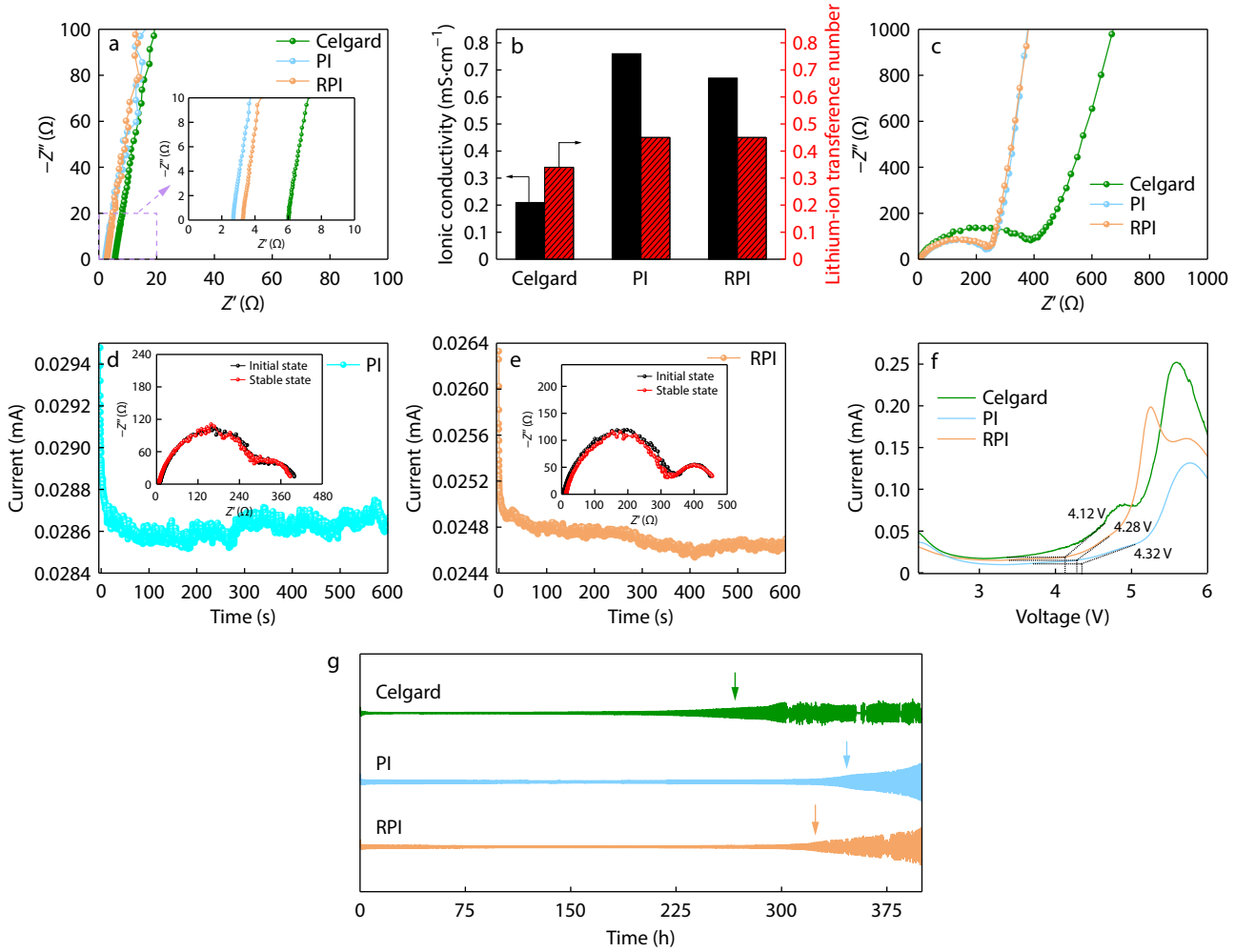

Fig. 9 (a) Nyquist plots of Celgard 2500, PI, and RPI separators, with insets showing magnified views; (b) The ionic conductivity and lithium-ion transference number of different separators; (c) EIS curves of Celgard 2500, PI, and RPI separators; Chronoamperometry and AC impedance plots of PI (d), and RPI (e) separators by assembling Li/separator/Li cells; (f) Linear sweep voltammograms were obtained for SS (stainless steel)//separator//Li cells assembled with different separators at a sweep rate of 5 mV·s^{-1}; (g) The cyclic performance of the Li/separator/Li at a current density of 1 mA·cm^{-2} for Celgard 2500, PI and RPI separators.

Table 1 Electrochemical performance data of different separators.

	Thickness (μm)	I_0 [a] (mA)	I_s [b] (mA)	R_0 [c] (Ω)	R_s [d] (Ω)	R_b [e] (Ω)	σ [f] (mS·cm^{-1})	t^+ [g]	R_{SEI} [h] (Ω)	Potential [i] (V)
Celgard	25	0.01829	0.01741	515	482	5.97	0.21	0.34	426	4.12
PI	40	0.02947	0.02860	312	289	2.68	0.76	0.45	264	4.32
RPI	43	0.02632	0.02461	340	318	3.27	0.67	0.45	274	4.28

[a] I_0 represents the initial currents; [b] I_s represents the steady-state currents; [c] R_0 represents the initial interfacial resistance; [d] R_s represents the steady-state interfacial resistance; [e] R_b represents the volume resistance; [f] σ represents the ionic conductivities calculated by Eq. S3 (in ESI); [g] t^+ represents the lithium-ion transference numbers calculated by Eq. S(4) (in ESI); [h] R_{SEI} represents the interface resistances; [i] Potential represents the oxidation potentials.

https://doi.org/10.1007/s10118-026-3730-6

which were significantly lower than those of the Celgard 2500 separator (426 Ω) (Fig. 9c). The lithium-ion transference numbers (t^+) of coin cells with a Li//separator//$LiCoO_2$ configuration assembled using Celgard 2500, PI, and RPI separators were determined by chronoamperometry combined with AC impedance spectroscopy, and the values were 0.34, 0.45, and 0.45, respectively (Figs. 9b, 9d and 9e, Fig. S3 in ESI, Table 1). In summary, the RPI separator exhibited a structural morphology similar to that of the PI separator, resulting in comparable porosity and overall performance. Therefore, both separators exhibited similar ionic conductivities and lithium-ion transference numbers.

For $LiCoO_2$-based batteries, a higher oxidation potential enhances discharge capacity and ensures reliable battery operation. As shown in Fig. 9(f), the oxidation potentials of the PI (4.32 V) and RPI (4.28 V) separators were comparable and both were higher than that of the Celgard 2500 separator (4.12 V). This indicates that the RPI separator exhibits electrochemical stability comparable to that of the PI separator and superior to that of conventional commercial membranes. Fig. 9(g) presents the cycling performance of symmetric cells assembled with Celgard 2500, PI, and RPI separators. The cell containing the RPI separator exhibited high stability and maintained consistent operation until noticeable potential fluctuations appeared after 320 cycles. Although the cycle life of the RPI-based cell (320 cycles) was slightly lower than that of the PI-based cell (340 cycles), it significantly outperformed the cell equipped with a commercial Celgard 2500 separator (250 cycles). These results indicate that the recycled RPI separator retains promising long-term cycling stability.

Battery Performance Based on RPI Separators

To evaluate the performance of the separator, coin-type half-cells with Li//separator//$LiCoO_2$ configurations were assembled and tested. The rate capabilities of the cells assembled with Celgard 2500, PI, and RPI separators are shown in Fig. 10 and Table S4 (in ESI). It is noteworthy that the discharge capacities of the cells containing PI and RPI separators at the second 0.2 C rate were 173.30 and 172.26 mAh·g^{-1}, respectively, with capacity retention ratios exceeding 97%. Moreover, the cells assembled with the PI and RPI separators exhibited similar discharge capacities across various current densities, and both outperformed the cells assembled with the Celgard 2500 separators. This improved performance is primarily attributed to the high-porosity structure resulting from the overlapping nanofiber structure and the highly polar nature of the polyimide molecular chains, which facilitate lithium-ion transport at high current densities. Moreover, the RPI separator possessed good mechanical strength and thermal stability, ensuring safe operation and cycling stability under high-rate conditions. Overall, the RPI separator obtained in this work exhibits structural morphology and electrochemical performance comparable to those of the conventionally prepared PI separator, endowing it with a similarly high discharge capacity and excellent rate capability.

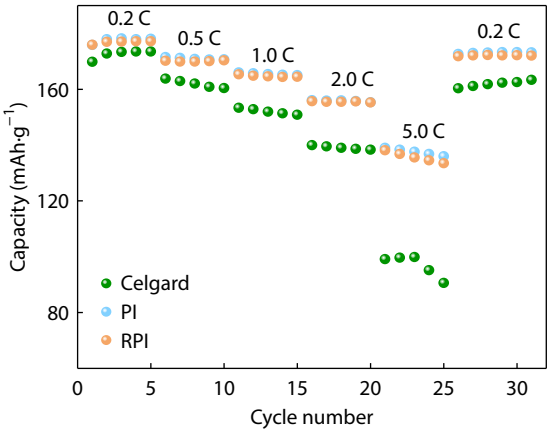

Fig. 10 Rate capability of Celgard 2500, PI and RPI separators (0.2–5.0 C).

The cycling performances of the batteries at various current densities are shown in Fig. 11 and Figs. S4–S6 (in ESI). After 100 cycles at 0.5 C, the discharge capacities of the cells assembled with Celgard 2500, PI, and RPI separators were 97.47, 119.29 and 118.01 mAh·g^{-1}, respectively. Under 2.0 C cycling for 100 cycles, the corresponding capacities were 11.10, 92.22, and 87.10 mAh·g^{-1}, respectively. The capacity retention, defined as the ratio of the discharge capacity at the 100th cycle to that of the first cycle, was calculated for each cell. At 0.5 C, the capacity retentions of the Celgard 2500, PI, and RPI cells were 98.64%, 99.82%, and 100.06%, respectively; at 2.0 C, they were 94.43%, 99.78%, and 99.72%, respectively. These cycling results demonstrate that the RPI lithium-ion battery exhibits long-term cycling stability comparable to that of the PI-based battery, and outperforms the battery equipped with the Celgard 2500 separator.

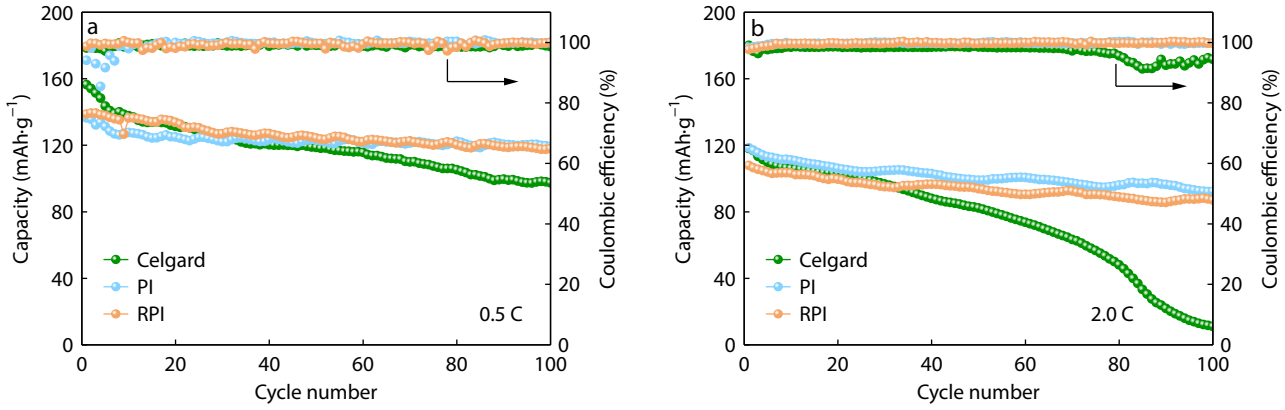

Fig. 11 Cycling performance and Coulombic efficiency at (a) 0.5 C, (b) 2.0 C for different separators.

https://doi.org/10.1007/s10118-026-3730-6

CONCLUSIONS

This paper presents a method for recycling waste polyimide (rPI) films generated during industrial production and reusing them to fabricate lithium-ion battery separators. Specifically, rPI films were efficiently recovered at room temperature using a LiOH solution to obtain a poly(amic acid)-polyimide (PAA-PI) precursor solution, which was then converted into high-performance nanofiber separators *via* electrospinning. The resulting recycled polyimide (RPI) separators exhibited no significant differences in morphology, chemical structure, mechanical properties, or thermal stability compared with conventional PI separators prepared by the traditional two-step method. Moreover, batteries assembled with RPI separators demonstrated electrochemical performances comparable to those using pristine PI separators, and both outperformed cells incorporating the commercial Celgard 2500 separator. Building on this, the chemically controlled ring-opening approach developed in this study enables the conversion of non-dissolvable and non-meltable recycled polyimide into a soluble PAA-PI solution. Similar to conventional PAA precursors, this recycled solution can be further processed into various polyimide materials with different morphologies, such as films or other configurations, while retaining satisfactory performance. Thus, beyond offering a strategy to reduce the manufacturing cost of polyimide-based separators, this work also enables the high-value reutilization of industrial polyimide waste, highlighting the advantages of a green and economically viable process with a simple operation.

Conflict of Interests

The authors declare no interest conflict.

Electronic Supplementary Information

Electronic supplementary information (ESI) is available free of charge in the online version of this article at http://doi.org/10.1007/s10118-026-3730-6.

Data Availability Statement

The data supporting the findings of this study are available from the corresponding author upon reasonable request.

ACKNOWLEDGMENTS

This work was financially supported by the Guangdong Provincial Department of Science and Technology (No. 2024B0101120001) and Shenzhen Municipal Bureau of Science and Technology Innovation (No. KJZD20240904170759001), National Key R&D Program of China (No. 2022YFB3806600), and the National Natural Science Foundation of China (Nos. U20A20255 and 52203286).

REFERENCES

1 Kothavade, P.; Kafi, A.; Shanmuganathan, K.; Bateman, S. High performance polyimides for additive manufacturing: a critical review. *Prog. Polym. Sci.* **2025**, *172*, 102055.
2 Peng, K.; Yang, X.; Du, B.; You, Y.; Zahidul Islam, M.; Abdullaev, A.; Fu, Y.; Dai, H. Development of flexible, robust, freestanding PTFE fiber film/PTFE particles-fluorinated polyimide hierarchical sandwich composites with ultra-low dielectric constant for high-frequency applications. *Compos. Commun.* **2025**, *57*, 102461.
3 Fu, Z.; Yu, D.; Xue, T.; Zhang, X.; Fan, W. 3D printed polyimide-based composite aerogels with shape memory and thermal insulation properties. *Compos. Commun*. **2025**, *56*, 102335.
4 Zhang, Q.; Wang, X.; Hu, X.; Yang, D.; Wei, H.; Cao, X.; Hou, Y.; Wang, J. Green synthesis of fluorine-containing polyimide aerogels toward passive daytime radiative cooling for energy saving. *Compos. Commun.* **2025**, *57*, 102450.
5 Chen, Y.; Liu, Y.; Min, Y. Innovative polyimide modifications for aerospace and optoelectronic applications: synergistic enhancements in thermal, mechanical, and optical properties. *ACS Appl. Mater. Interfaces* **2025**, *17*, 16016−16026.
6 Aghababaei Tafreshi, O.; Saadatnia, Z.; Ghaffari-Mosanenzadeh, S.; Rastegardoost, M. M.; Zhang, C.; Park, C. B.; Naguib, H. E. Polyimide aerogel fiber bundles for extreme thermal management systems in aerospace applications. *ACS Appl. Mater. Interfaces* **2024**, *16*, 54597−54609.
7 Bai, F.; Jiang, Y.; Li, X.; Dong, J.; Zhao, X.; Zhang, Q. Fabrication and characteristics of bend-durable, colorless transparent polyimide films for flexible display cover applications. *Acta Polymerica Sinica* (in Chinese) **2024**, *55*, 1393−1404.
8 Zhang, T.; Yu, J.; Wang, S.; Chai, Y.; Jiang, S.; An, H.; Sun, R.; Li, B. Synthesis and properties of heat-resistant polyimides films containing crosslinkable group-tetrafluorostyrene. *Chinese J. Polym. Sci.* **2025**, *43*, 863−874.
9 Ruan, K.; Guo, Y.; Gu, J. Liquid crystalline polyimide films with high intrinsic thermal conductivities and robust toughness. *Macromolecules* **2021**, *54*, 4934−4944.
10 Maeda, H.; Liang, Y.; Hosoya, R.; Marui, R.; Yoshida, E.; Chen, Y.; Hatakeyama-Sato, K.; Nabae, Y.; Nakagawa, S.; Morikawa, J.; Tokita, M.; Sawada, R.; Ando, S.; Hayashi, Y.; Yoshida, R.; Furuya, H.; Hayakawa, T. Smectic liquid crystalline poly(ester imide)s with low dielectric dissipation factors for high-frequency applications. *Polym. J.* **2025**, *57*, 665−677.
11 Sajjad, L.; Ustad, R. E.; Chavan, V. D.; Sheikh, Z. A.; Avatare, A. T.; Khan, M. F.; Kim, H.; Kim, D. Recent progress and challenges of photosensitive polyimides in advanced packaging: Technology beyond Limit. *Eur. Polym. J.* **2025**, *239*, 114302.
12 Hou, T.; He, C.; Lin, Y.; Zhao, Y.; Ding, L. Low-temperature curing polyimide composites with low coefficient of thermal expansion for high-temperature electronic packaging. *Nano Research* **2025**, *18*, 94907310.
13 Lu, Z.; Sui, F.; Miao, Y.; Liu, G.; Li, C.; Dong, W.; Cui, J.; Liu, T.; Wu, J.; Yang, C. Polyimide separators for rechargeable batteries. *J. Energy Chem.* **2021**, *58*, 170−197.
14 Li, A.; Rong, Z.; Yuan, B.; Cheng, F.; Zhang, W. Crosslinked polyimides as cathodes for lithium-ion batteries. *ACS Appl. Energy Mater.* **2023**, *6*, 1862−1870.
15 Srinivaas, M.; Lee, Y.-Y.; Busireddy, M. R.; Hsu, C.; Devi S, B.; Boddula, R.; Kamble, G. S.; Chang-Chien, G. Polyimides in next-generation energy devices: applications in Li-ion batteries to solar cells. *J. Power Sources* **2025**, *641*, 236780.
16 Huang, H.; Chen, K.; Li, C.; Zhou, Z.; Wang, W.; Deng, B.; Liu, S.; Qian, C.; Yue, M.; Chi, Z.; Xu, J.; Zhang, Y. Zwitterion grafted polyimide separator for improving lithium-ion transport and its application in $LiCoO_2$ batteries. *Chem. Eng. J.* **2024**, *481*, 148577.
17 Olifirov, L.; Kaloshkin, S.; Zadorozhnyy, M.; Zadorozhnyy, V.; Tcherdyntsev, V.; Danilov, V. Recycled moulded polyimide materials obtained by high-energy ball milling. *J. Appl. Polym. Sci.*

Graphical Abstract

Low-cost Preparation of High-performance Polyimide Separators: High-value Application of Recycled Polyimide Films

Ying-Hua Sha, Zi-Hao Huang, Jia-Shu Lin, Yan-Wei He, Chu-Ying Li, Hai-Tao Huang, Si-Wei Liu, and Yi Zhang

Sun Yat-sen University; Jiaying University; Wuxi Shunxuan New Materials Co., Ltd.

Lithium hydroxide catalyses the partial ring-opening of imide groups in waste polyimide (PI) films, yielding a soluble poly(amic acid) (PAA)-PI precursor, and electrospun into separators, enabling high value application of recycled PI films.

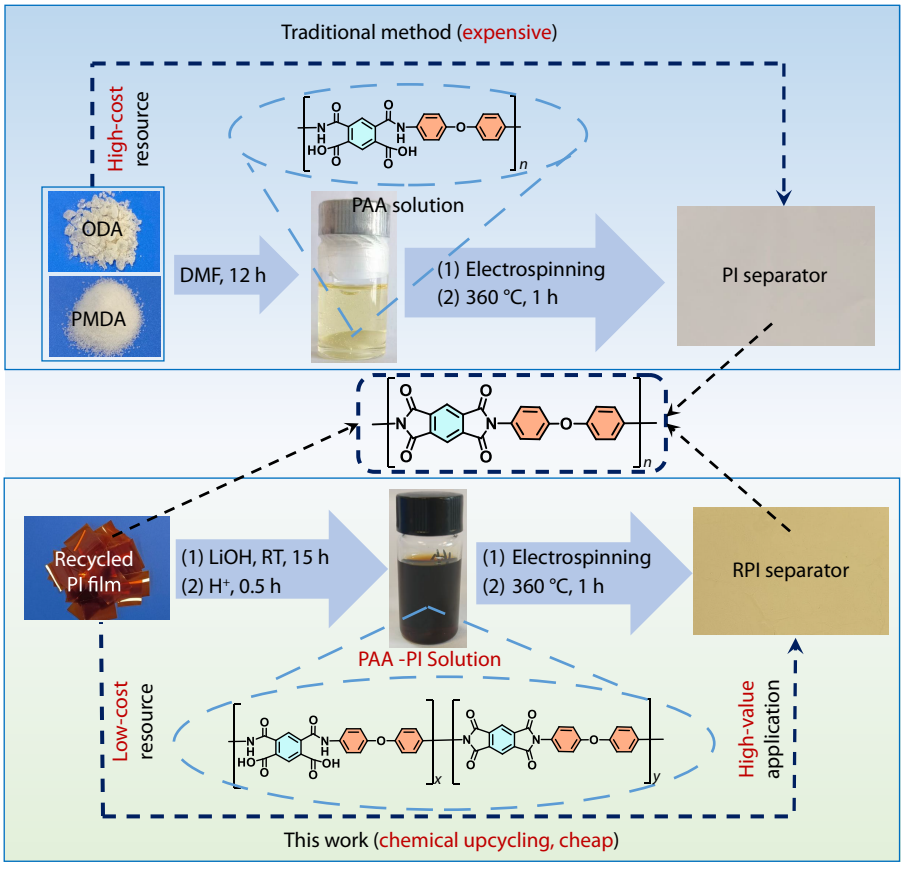

Chinese J. Polym. Sci., 2026 *https://doi.org/10.1007/s10118-026-3730-6*

2018, *135*, 46733.

18 Olifirov, L.; Kaloshkin, S.; Ergin, K.; Tcherdyntsev, V.; Danilov, V. Solid-state recycling of polyimide film waste. *J. Appl. Polym. Sci.* **2013**, *127*, 2960–2968.

19 Ding, M.; Deng, Z.; Huang, Z.; Wang, Y. Recovery of polyimide waste film by mechanical method to improve the heat fade resistance of BPR matrix friction composites. *Wear* **2022**, *502–503*, 204398.

20 Kumagai, S.; Hosaka, T.; Kameda, T.; Yoshioka, T. Pyrolysis and hydrolysis behaviors during steam pyrolysis of polyimide. *J. Anal. Appl. Pyrolysis* **2016**, *120*, 75–81.

21 Kumagai, S.; Hosaka, T.; Kameda, T.; Yoshioka, T. Steam pyrolysis of polyimides: effects of steam on raw material recovery. *Environ. Sci. Technol.* **2015**, *49*, 13558–13565.

22 Stephans, L. E.; Myles, A.; Thomas, R. R. Kinetics of alkaline hydrolysis of a polyimide surface. *Langmuir* **2000**, *16*, 4706–4710.

23 Tian, Z.; Zhao, Q.; Liu, X.; Wang, Y.; Zhao, J.; Wang, Y.; Hou, X. Efficient aminolysis of polyimide for chemical recovery of flexible printed circuit boards. *ACS Sustain. Chem. Eng.* **2023**, *11*, 11590–11600.

24 Chen, H.; Liu, X.; Zhang, S.; Xu, S.; Fu, T.; Wang, Y. Full recovery of polyimide wastes into high-value products through break and reconstruction of imide ring. *Adv. Sci.* **2025**, *12*, 2414416.

25 Zhang, F.; Wang, F.; Wei, X.; Yang, Y.; Xu, S.; Deng, D.; Wang, Y. From trash to treasure: chemical recycling and upcycling of commodity plastic waste to fuels, high-valued chemicals and

advanced materials. *J. Energy Chem.* **2022**, *69*, 369–388.
26 Chen, H.; Liu, X.; He, Q.; Zhang, S.; Xu, S.; Wang, Y. Upcycling waste thermosetting polyimide resins into high-performance and sustainable low-temperature-resistance adhesives. *Adv. Mater.* **2024**, *36*, 2310779.
27 Cai, S.; Wang, Y.; Guo, Z.; Deng, X.; Liu, D.; Beiyuan, J.; Lv, D.; Peng, J.; Huang, L.; Cha, R.; Yuan, W. Mechanochemically catalytic upcycling of PET wastes toward aerogels for thermal insulation. *Chem. Eng. J.* **2024**, *497*, 154583.
28 Honma, T.; Sato, T. Hydrolysis Kinetics of PMDA/ODA polyimide for monomer recovery using sodium hydroxide in high-temperature water. *J. Supercrit. Fluids* **2020**, *166*, 105037.
29 Perry, D.; Mamlouk, M. Probing mass transport processes in Li-ion batteries using electrochemical impedance spectroscopy. *J. Power Sources* **2021**, *514*, 230577.

https://doi.org/10.1007/s10118-026-3730-6